Über ein neues Radiofrequenz-Mikrowellen-Doppelresonanzexperiment

R. SCHWARZ * und H. DREIZLER

Abteilung Chemische Physik
im Institut für Physikalische Chemie der Universität Kiel

(Z. Naturforsch. **27 a**, 708—709 [1972]; eingegangen am 17. Januar 1972)

Die bisherigen Radiofrequenz-Mikrowellendoppelresonanzexperimente hatten ein Rotationstermschema eines Moleküls als Basis, bei dem die Auswahlregeln Übergänge im Radiofrequenz- und Mikrowellengebiet, ausgehend von einem Niveau, zulassen. Als Pumpe wurde die Radiofrequenz, als Signal die Mikrowelle verwendet [1–3].

Hier berichten wir über ein Experiment, bei dem sich die Moleküle in einem statischen elektrischen Feld E_{st} befinden. Jedes Rotationsniveau spaltet dabei durch Stark-Effekt in eine Anzahl von „Stark"-Niveaus auf, wie in Abb. 1 für den Übergang $2_{11}-2_{12}$ $\nu_0 = 14\,488{,}65$ MHz von Formaldehyd, H_2CO, illustriert wird. Man pumpt mit einer Radiofrequenz, die senkrecht zu E_{st} polarisiert ist, zwischen den Niveaus $|M|=1$ und $|M|=2$. Die Mikrowelle ist parallel zu E_{st} polarisiert. Beobachtet werden Doppelresonanzsignale bei den Frequenzen ν_1 und ν_2, bei denen beim Stark-Effektmodulationsverfahren die Stark-Satelliten erscheinen, wenn die Amplitude der Stark-Rechteckspannung gleich E_{st} ist. Bei der Linienfrequenz ν_0 ist kein Signal, wie Abb. 2 zeigt.

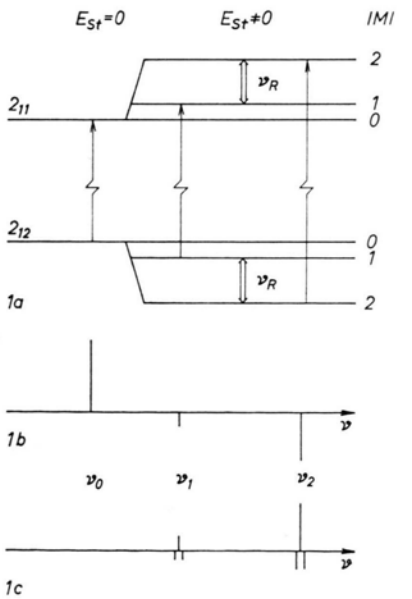

Abb. 1 a. Termschema für das „Stark"pumpen. Niveaus 2_{11} und 2_{12} von H_2CO. ↑ Mikrowellenübergang; ⇕ Pumpübergang.

Abb. 1 b. Linienbild bei Stark-Effektmodulation.

Abb. 1 c. Linienbild bei „Stark"pumpen.

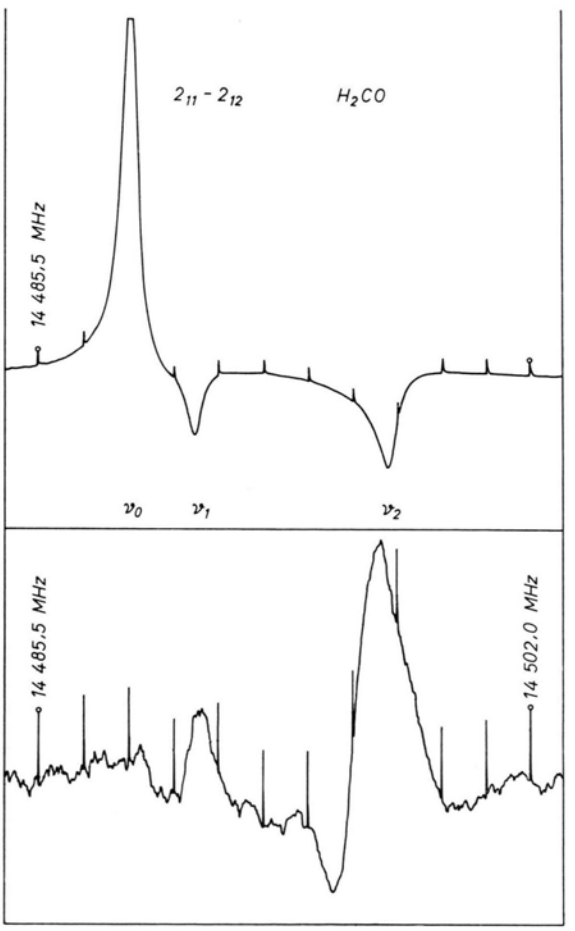

Abb. 2. Registrierungen zur Illustration von Abb. 1 b und 1 c. Bei der oberen, 1 b entsprechenden Registrierung erscheint der $|M|=2$-Stark-Satellit mit einer verfälschten Intensität. Die Ursache ist noch nicht bekannt.

Für das Experiment wurde eine spezielle Mikrowellenabsorptionszelle gebaut, deren Querschnitt in Abb. 3 angegeben ist. In einer gewöhnlichen Stark-Absorptionszelle ist zu beiden Seiten des Septums je eine Lecher-Leitung für die Radiofrequenz angebracht. Wesentlich ist, daß sie auf einem Potential $E_{st}/2$ gehalten werden. Das RF-Signal wird aufaddiert.

Eine wesentliche Nutzanwendung dieses Effekts in der Mikrowellenspektroskopie wird darin liegen, daß

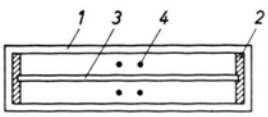

Abb. 3. Querschnitt durch die Absorptionszelle. 1 Hohlleiter; 2 Teflonisolierung; 3 Stark-Septum; 4 Lecher-Leitung.

* Teil der Dissertation.
Sonderdruckanforderungen an Prof. Dr. H. DREIZLER, Institut für Physikalische Chemie der Universität Kiel, Abteilung Chemische Physik, *D-2300 Kiel*, Olshausenstr. 40–60.

störende Linien mit hohen Drehimpulsquantenzahlen J unterdrückt werden, wenn das statische Feld E_{st} und die Radiofrequenz ν_R auf einen Übergang mit niedrigem J abgestimmt ist, da wegen der meist geringeren Stark-Aufspaltung von Niveaus mit höherem J ein Doppelresonanzeffekt dort nicht möglich ist. Bei Mikrowellenspektren mit einer hohen Liniendichte kann dadurch die Zuordnung erleichtert werden. Auch eine genaue Dipolmomentbestimmung erscheint möglich.

Details des Effekts, andere Zellgeometrien und Anwendungen werden zur Zeit untersucht und später mitgeteilt.

Der Werkstatt des Instituts danken wir für die Ausführung der mechanischen Arbeiten, der Deutschen Forschungsgemeinschaft und dem Fonds der Chemie für Personal- und Sachmittel.

[1] S. H. Autler u. C. H. Townes, Phys. Rev. **100**, 703 [1955].
[2] F. J. Wodarczyk u. E. B. Wilson jr., J. Mol. Spectrosc. **37**, 445 [1971].
[3] R. Schwarz u. H. Dreizler, Vortrag: RF-MW-Double Resonance, Colloquium on High Resolution Molecular Spectroscopy, Dijon, Sept. 1971 — und unveröffentlicht.

ESR, Dielectric and Optical Absorption of Manganese (II) Chloro Complexes in DMF and DMA Solution

H. Pirot and M. Stockhausen

Institut für Physik, Abteilung Mikrowellenphysik
Universität Mainz

(Z. Naturforsch. **27 a**, 709—711 [1972]; received 14 February 1972)

The tetrahedral complex $MnCl_4^{2-}$ in solution exhibits a characteristic absorption spectrum (yellow instead of pink colour) [1, 2] as well as a characteristic ESR spectrum with a smaller hfs splitting than other Mn^{2+} complexes [3]. We have investigated solutions containing tetrahedral complexes, among others, to find out if characteristic optical and ESR spectra appear together or if there are differences to distinguish further between special complex species. The experiments were carried out with solutions of hydrated manganous chloride ($MnCl_2 \cdot 4\,H_2O$) in dimethylformamide (DMF) and dimethylacetamide (DMA) in a medium concentration range (0.05 ... 0.5 mol/l). Solutions in dimethylsulfoxide (DMSO) give results similar to DMF. Hydrated salt was used because of the stability of the solutions in contact with air.

In addition to ESR and optical spectra, dielectric absorption was used as third tool indicating but special complexes. The data, as shown in Fig. 1, are divided by the manganese concentration c to indicate the concentration dependence of the fraction of complex species deteted by the various methods.

Optical absorption of the yellow solutions was measured in the visible and near UV region. The maxima are the same (at 22 550, 23 400 and 28 100 cm^{-1}) as reported for the tetrahedral $MnCl_4^{2-}$ and mixed tetrahedral species [1, 2]. Beer's law is not obeyed. At higher concentrations, nevertheless, the molar extinction E/c depends only slightly on the concentration.

Dielectric absorption measurements were made in the 300 to 1800 MHz range. From the total imaginary part of the dielectric constant (ε'') was substracted the extrapolated conductive part (ε_1'') and the contribution of the pure solvent (ε_3''). The remaining ε_2'' is due to absorption by ionic dipoles alone [4]. Solutions of pure water, corresponding to the water concentration of the hydrated salt, show negligible ε_2'' in the frequency band used.

Taking into account measurement errors, ε_2'' follows an absorption curve broader than a Debye curve [approximately a Fröhlich curve [5] with $\ln(\tau_1/\tau_2) = 2.5$], indicatinig several relaxation times or a continuous distribution. $\varepsilon''_{2\max}/c$ is only slightly concentration dependent in both solvents. The mean relaxation time τ is 280 ($\pm$ 50) ps im DMF, also independent of concentration, while in DMA $\tau \approx 280$ ps at 0.1 mol/l and about 200 ps at 0.5 mol/l.

The ESR spectra of both solutions are quite different. In DMF, at low concentrations the spectrum is well resolved and exhibits more than the usual six lines (Fig. 2) [6]. In the whole concentration range it may be described as superposition of two spectra with equal g-factor and intensities, but different hfs splitting ($A_2 = 0.84\ A_1$). The "anomalous" splitting A_2 is in agreement with the splitting observed on $MnCl_4^{2-}$ complexes [3]. — In DMA, at low concentrations the well resolved spectrum consists of six hfs components of equal linewidth, with the same splitting A_1 as observed in other manganous solutions (e. g. water, $A_1 = 95$ Oe). — Adding excess chloride (with diamagnetic cations), both spectra approach a uniform anomalous spectrum with A_2.

Related to the concentration, the signal intensity is relatively too weak in both solutions. From intensity and observed linewidth one deduces the relative spin number N/N_0, which is the fraction of species detected by ESR. N/N_0 increases with increasing concentration, especially in DMF solutions. At higher concentrations an additional broad (and therefore very weak) background spectrum becomes indicable, which may be attributed to the lacking spins, not represented by N/N_0.

The limiting linewidth at dilution, ΔH, in DMF is the same as with other salts in this solvent (e. g. nitrate, perchlorate): $\Delta H/A_1 = 0.26$ (for the smallest line). In DMA, the hfs components of chloride ($\Delta H/A_1 = 0.38$) are somewhat broader than those of other salts (0.31).

Reprint requests to Dr. M. Stockhausen, Institut für Physik, Universität Mainz, *D-6500 Mainz.*

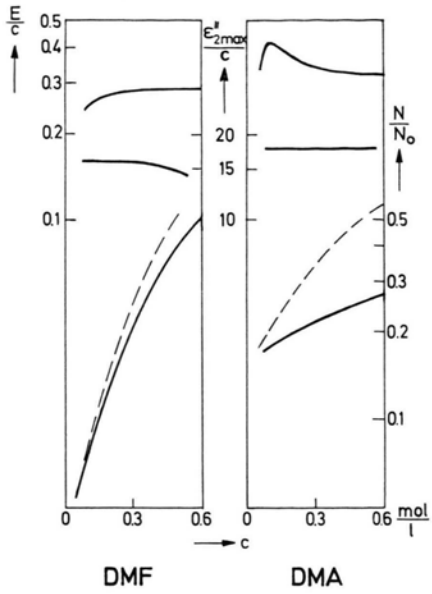

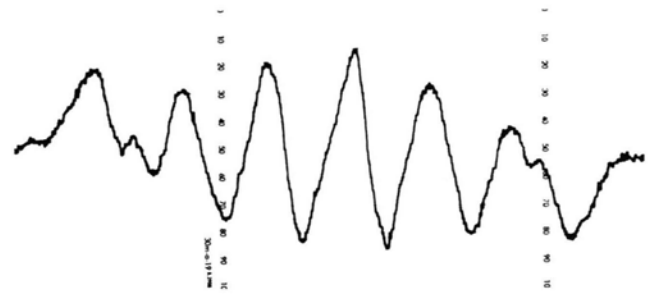

Fig. 2. ESR spectrum of 0.06 mol/l $MnCl_2 \cdot 4\,H_2O$ in DMF.

← Fig. 1. Decadic extinction coefficient, E/c, at 28 000 cm^{-1} (top); Maximum of ionic dipole part of dielectric absorption, ε''_{2max}/c (middle); Spin fraction, N/N_0, of resolved ESR spectra (below); versus manganese concentration c. ———: $MnCl_2 \cdot 4\,H_2O$; — — —: $MnCl_2$.

For comparison, Fig. 1 shows also ESR results on water-free salts, with a noteworthy increase of the detected spin fraction in the DMA solution.

The discussion is based on the assumption of an equilibrium between various species, belonging to at least two coordination types. Their ionic composition may be represented by

$$\begin{aligned} &A,\ AB,\ AB_2 \ldots && \text{octahedral,} \\ &\ldots\ AB_3,\ AB_4 && \text{tetrahedral.} \end{aligned}$$

(The free sites of the first coordination sphere may be occupied by solvent or water molecules. Coordination of anions in the second sphere is also possible, at least in the octahedral case.) The three measuring methods are selective for special species: The "yellow" optical spectrum detects all tetrahedral species (also with mixed coordination [2]). The dielectric absorption detects species with an electric moment, thus all except A and AB_4. Complementary to the dielectric measurements, the ESR spectrum (its well resolved part) detects species of high symmetry, namely A and AB_4.

The initial question is to be answered as follows: "Yellow" spectrum and "anomalous" hfs splitting are not necessarily related. In spite of a similar optical spectrum, both solutions show different ESR spectra and different concentration dependence of extinction and spin fraction N/N_0.

To describe the species in the solution, mention must be made of the steep decrease of equivalent conductivity with increasing concentration, far below the concentrations used here, which (as well as the spin number) proofs the fraction of species A to be small. — Since dielectric relaxation may be attributed to rotational orientation, the mean effective radius of the relaxing units may be estimated from the relaxation time by comparison with other dielectric data [7]; it is found to be about 6.5 Å. Therefore the dielectrically detected species must be solvated. The absorption curves (ε'' versus frequency) indicate that different types may be present, but a detailed analysis would not be significant. Since the electric moments of the various polar species as well as their relaxation times may be in the same order of magnitude, we conclude from the ε''_{2max} values, as a rough approximation, the total fraction of these species to be nearly concentration independent. The same follows from optical data (in a certain concentration range) for the total fraction of tetrahedral species. Thus AB_4 is the only species of the above list to be detected by ESR, and for balance its spin fraction should also be only slightly concentration dependent, in contrast to our results.

Therefore the observed ESR spectrum has to be attributed to an additional species, not listed above. We conclude from the nearly 1 : 1 composition of the spectrum in DMF that it may be a higher (presumably solvated) complex of the $A \cdot AB_4$ ionic type, e. g. composed of two molecules ($MnCl_2$) in a way that one cation is surrounded by four anions, the second cation remaining outside the tetrahedron. Such a complex would exhibit "yellow" optical absorption as well as dielectric absorption. This assumption is supported by the ESR behaviour in DMA: In nearly all other cases of well resolved Mn^{2+} solution spectra, the outer hfs components are broadened because they are composed from five lines, which do not coincide perfectly. But in our case, all six hfs lines have equal linewidth. This may be the result of a slow spin exchange process (exchange frequency about 30 MHz) or a superexchange process via Cl^-. A possibility for those exchange processes is given by the proposed dimeric complex.

We are indebted to Prof. Dr. G. KLAGES for helpful discussions.

[1] S. BUFFAGNI and T. M. DUNN, Nature London **188**, 937 [1960]. — F. A. COTTON, D. M. L. GOODGAME, and M. GOODGAME, J. Amer. Chem. Soc. **84**, 167 [1962].
[2] C. FURLANI and A. FURLANI, J. Inorg. Nucl. Chem. **19**, 51 [1961].
[3] S. I. CHAN, B. M. FUNG, and H. LÜTJE, J. Chem. Phys. **47**, 2121 [1967]. — H. LEVANON and Z. LUZ, J. Chem. Phys. **49**, 2031 [1968].
[4] R. POTTEL, Ber. Bunsenges. Phys. Chem. **69**, 363 [1965].
[5] K. KREUTER, Z. Naturforsch. **23 a**, 1728 [1968].
[6] W. LOHMANN, C. F. FOWLER, W. H. PERKINS, and J. L. SANDERS, Nature London **209**, 908 [1966].
[7] F. HUFNAGEL, Z. Naturforsch. **25 a**, 1143 [1970].

Characteristics of a Tunable Travelling Wave Dye Ring Laser

G. MAROWSKY, L. RINGWELSKI, and F. P. SCHÄFER

Max-Planck-Institut für Biophysikalische Chemie
(Abteilung Laser-Physik)
Göttingen, West Germany

(Z. Naturforsch. **27 a**, 711—713 [1972]; received 21 February 1972)

A flashlamp pumped dye ring laser using 4 Abbé prisms of constant 90 degree deviation has been built. Travelling wave operation is obtained when the counterclockwise wave is fed back by a beam-splitting output prism. The laser emission offers remarkable frequency stability when narrowed down to a linewidth of 7 pm by the use of an intracavity solid Fabry-Perot etalon.

Introduction

Various methods are known for the achievement of tunable, narrowband emission from organic dye lasers [1–3]. By inserting frequency selective elements — based on dispersion, rotational dispersion or interferometry — into the cavity, the spectral output can be reduced from some ten nanometers to a fiew picometers. Tunable narrowband laser emission down to a linewidth of 50 pm was reported by SCHÄFER and MÜLLER [4] using a six-prism ring laser. In the present work, we describe the properties of a ring laser using 4 Abbé or Pellin-Broca prisms whose emission was additionally spectrally narrowed by the insertion of a Fabry-Perot etalon into the laser resonator.

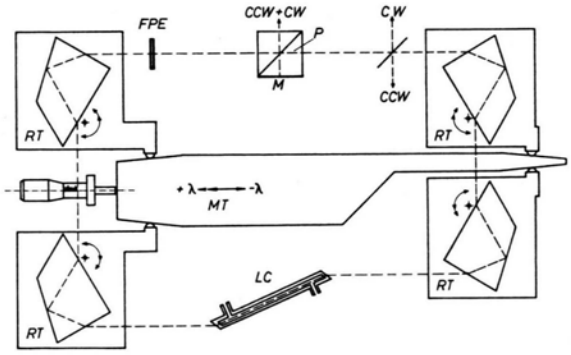

Fig. 1. Ring laser unit; LC: laser cuvette; RT: rotating prism table with Abbé prisms, axis and sense of rotation indicated; MT: movable table; FPE: Fabry-Perot etalon; P: beam splitting output prism with high reflectivity mirror M, for clarity the output prism has been rotated by 90° around the beam axis; G: glass sampling plate for separate measurement of CW and CCW output.

Dye Laser Construction

The flashlamp pumped dye laser consisted of a Brewster angled, 80 mm long, 2 mm internal diameter quartz glass dye cell within an elliptical cylinder reflector. It was optically pumped by a linear flashlamp (pump energy 200 J, ILC dye laser flashlamp type 4D3). The ring-shaped resonator (Fig. 1) was made of 4 highly dispersive (Schott SF 10 glass) Abbé prisms of constant 90° deviation arranged at Brewster's angle to avoid reflection losses. The wavelength tuning was achieved by simultaneous counter rotation of the 4 mechanically coupled prisms. To change the wavelength from 436 m to 656 nm a prism rotation of 2.4° was necessary [5]. One advantage of the arrangement lies in the fact that the lateral displacement of the beam does not exceed 0.1 mm for a 220 nm wavelength interval. In addition, only a single prism set is necessary for tuning throughout the whole visible and near infrared spectral region. The simultaneous counter rotation of the 4 prisms was accomplished by means of the linear motion of a table equipped with roller bearings of high mechanical precisions.

Power was extracted from the ring laser by a dielectric beam splitting prism of 25% reflectivity. Three faces of this prism were antireflection coated whereas the fourth face was provided with a high reflectivity coating. The latter served to increase the output and to force the laser into unidirectional, travelling wave operation, by partially reflecting the counterclockwise (CCW) wave back onto itself [6]. For further spectral narrowing of the laser emission an intracavity solid Fabry-Perot etalon (FPE) was employed. It consisted of a multilayer coated quartz plate of 0.25 mm thickness with a free spectral range of about 0.58 nm at 660 nm (further details cf. [7]) * and had a reflectivity of 78%. By tilting the FPE around a horizontal axis, the emision wavelength could be shifted by a few picometers.

Results

Figure 2 shows the peak output power obtained from various dyes within the wavelength range 550 nm to

* The Fabry-Perot etalon was kindly put at our disposal by Dr. W. SCHMIDT, Carl Zeiss, Oberkochen.

650 nm. The data were taken at a constant pump energy of 200 J (1 μF, 20 kV) ** and with travelling wave operation of the laser. A far field photograph of the output showed a beam divergence of 1.2 mrad (full

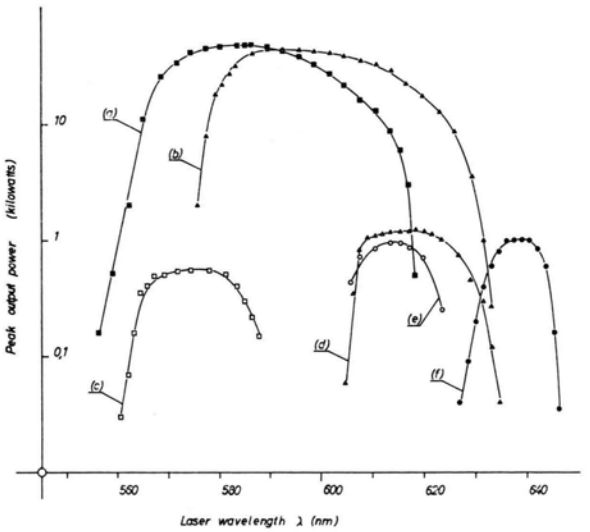

Fig. 2. Tuning range and peak output power for different dye solutions at constant pump energy of 200 J; (a) rhodamine 6G, $2 \cdot 10^{-4}$ molar in methanol; (b) rhodamine 6G, $2 \cdot 10^{-4}$ molar in water with cyclooctatetraene ($2 \cdot 10^{-4}$ molar) and Ammonyx^{R} (2.5%) added; (c) 6-acetylaminopyrene-1,3,8-trisulfonate, $2 \cdot 10^{4}$ molar in water; (d) sulforhodamine B, $3 \cdot 10^{-4}$ molar in methanol; (e) rhodamine B, $3 \cdot 10^{-4}$ molar in methanol; (f) rhodamine 6G, $7 \cdot 10^{-4}$ molar and cresyl violet, $8 \cdot 10^{-5}$ molar in methanol, according to (8).

angle at half-maximum intensity). The total pulse duration varied from 75 nsec (6-acetylaminopyrene-1,3,8-trisulfonate) to 1 μsec for rhodamine 6G. Insertion of the FPE reduced the spectral halfwidth of the emission from less than 1 nm to 7 pm. In contrast to the modal behavior of linear cavities, spectral analysis with an external interferometer revealed no marked or reproducible modal structure. The linewidth obtained by using the intracavity FPE was only weakly affected by variations of the pump energy. Using a $2 \cdot 10^{-4}$ molar solution of rhodamine 6G in methanol, the linewidth increased from 7 pm to 8 pm as the pump energy was raised from 22 J near threshold to 200 J.

The absence of a modal structure evidently contributed to the remarkable wavelength stability from shot to shot. The coarse adjustment by simultaneous prism rotation allowed a reproducible wavelength shift of as little as 0.15 nm. By tilting the FPE, the laser emission could be fine-tuned by 1 pm with an uncertainty of the spectral position of 0.5 pm. Figure 3 shows the fine-tuning by a series of interferograms. The analyz-

** Subsequently, the pumping efficiency was considerably increased by using a PEK-Labs flashtube, type XE 1-3. Peak output powers of 70 kV were obtained at a pump energy of 60 J (0.3 μF, 20 kV).

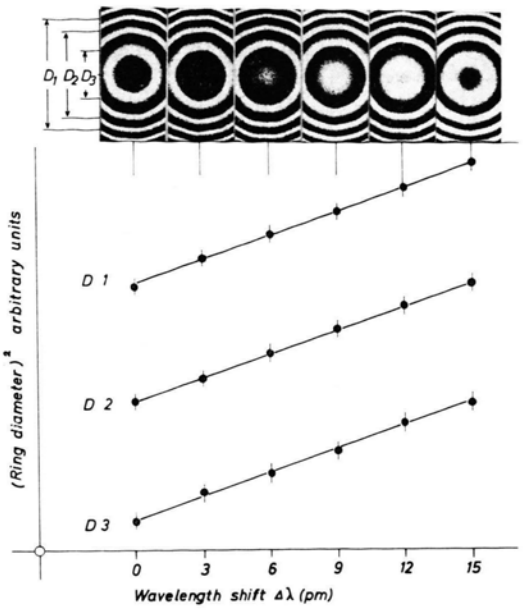

Fig. 3. Interferograms and results of densitometric analysis thereof showing fine tuning in steps of 3 pm.

ing Fabry-Perot interferometer had a plate spacing of 10 mm, corresponding to a free spectral range of 18 pm at 600 nm. The laser output remained practically constant when the FPE was inserted provided that the angle of incidence was kept within the interval 0.5° to 2.0°. For angles of incidence less than 0.5°, the high reflectivity coating acted as resonator mirrors, splitting the ring laser into a ring-shaped linear laser with the concomitant increase of the spectral bandwidth [4]. In the present experiments, the free spectral range of the intracavity FPE (0.58 nm) was less than the prism preselector bandwidth. Therefore, occasionally two lines of almost equal intensity were observed. In further experiments an FPE of 1 nm free spectral range will be used.

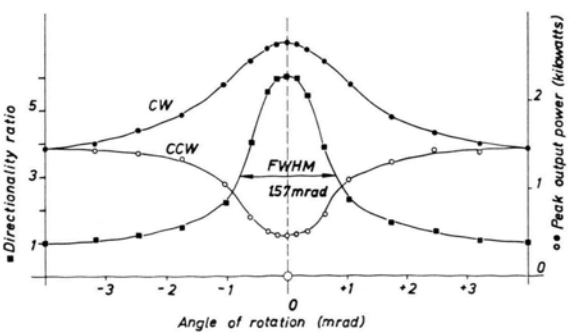

Fig. 4. Output power of clockwise (CW) and counterclockwise (CCW) traveling waves and resulting directionality ratio as a function of rotation of beam splitting output prism near feedback position.

The beam-splitting output prism was used to achieve travelling wave operation of the ring laser. By observing the far field, the clockwise (CW) and counterclockwise (CCW) travelling waves in the resonator could be brought into spatial coincidence by rotation of the beam-splitting prism. Figure 4 shows the output power of the CW and CCW emission and the resulting directionality ratio as a function of the angle of prism rotation. In the case of a symmetric position of the output prisms relative to the laser cuvette, as shown in Fig. 1, the directionality ratio (ratio of clockwise to counterclockwise output) was found to be 6 : 1. The output in the travelling wave mode of operation exceeded by 10% the sum of the uncoupled CW and CCW output. The directionality ratio was reduced to half its maximum value by rotating the prism from the central position to +0.8 or −0.8 mrad. This FWHM value of 1.6 mrad is almost equal to the above mentioned beam divergence angle. This property is the object of further investigation.

We thank Dr. M. PILTCH for a critical reading of the manuscript. The work was supported by the Fonds der Chemischen Industrie and the Deutsche Forschungsgemeinschaft.

[1] B. H. SOFFER and B. B. MCFARLAND, Appl. Phys. Letters **10**, 226 [1967].
[2] P. P. SOROKIN, J. R. LANKARD, and V. L. MORUZZI, Appl. Phys. Letters **15**, 179 [1969].
[3] D. J. BRADLEY, G. M. GALE, M. MOORE, and P. D. SMITH, Phys. Letters **26 A**, 378 [1968].
[4] F. P. SCHÄFER and H. MÜLLER, Opt. Commun. **2**, 407 [1971].
[5] L. RINGWELSKI, Dissertation, Universität Marburg 1971.
[6] M. HERCHER, M. YOUNG, and C. B. SMOYER, J. Appl. Phys. **36**, 3351 [1965].
[7] J. KUHL, G. MAROWSKY, P. KUNSTMANN, and W. SCHMIDT, Z. Naturforsch., paper accepted for publication [1972].
[8] W. SCHMIDT, W. APPT, and N. WITTEKINDT, Z. Naturforsch. **27 a**, 37 [1972].

Abklingzeiten und Radiolumineszenzausbeuten von Styrenlösungen PPO im Polymerisationsprozeß

M. GRODEL und Z. POLACKI

Physikalisches Institut der Technischen Hochschule, Gdańsk

(Z. Naturforsch. **27 a**, 713—715 [1972]; eingeg. am 22. November 1971)

In der Arbeit werden Szintillationszeiten und Radiolumineszenzausbeuten von Styrenlösungen PPO beim Polymerisationsprozeß mitgeteilt. Es wurde festgestellt, daß sich die Abklingzeit mit dem Konversionsgrad wie folgt ändert: der Anfang- und Endwert ist $\tau = 3{,}9 \cdot 10^{-9}$ s, dagegen beträgt der Maximalwert für den Konversionsgrad $\sim 50\%$ $\tau_{max} = 10^{-8}$ s.

Die Fluoreszenz von Styrollösungen einiger Luminophore während des Polymerisationsprozesses wurde bei Anregung mit γ-Strahlen von KRENZ [1] und von WEINREB und AVIVI [2] untersucht. Die Ergebnisse zeigten eine Änderung der Radio-Lumineszenzausbeute und der Übertragungsausbeute während des Polymerisationsprozesses. Weitere derartige Messungen [3, 4] lassen die Nützlichkeit solcher Untersuchungen für die Beurteilung des Einflusses der Polymerisationsbedingungen bei festen Polystyrollösungen erkennen. In der vorliegenden Arbeit wurden Abklingzeiten und Radiolumineszenzausbeuten während der Polymerisation von Styrollösungen mit 2.5-Phenyloxazol (PPO) gemessen.

1. Experimente

Styrol der Chemischen Werke Oświęcim (Polen), nagereinigt durch Destillation bei niederem Druck, und 2.5-Phenyloxazol (PPO) von Nuclear Enterprises, Edinburgh (G.-B.) (szintillationsrein) wurden in zylindrischen Pyrexbehältern (25 mm Durchmesser) einer thermischen Polymerisation unterzogen. Das Volumen der polymerisierten Substanz betrug 15 ml. Die relative Radiolumineszenzausbeute wurde a) aus dem mittleren

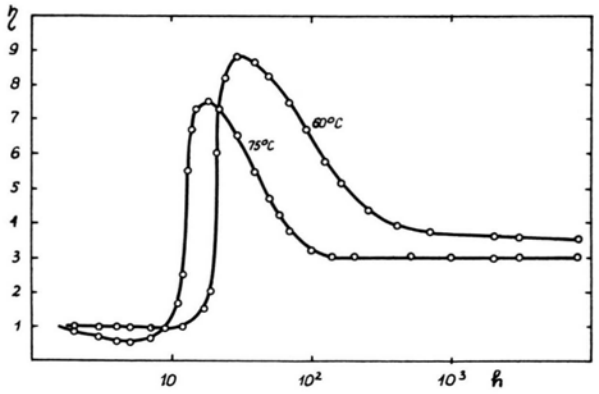

Abb. 1. Abhängigkeit der Radiolumineszenzausbeute (η) von der Polymerisationszeit (t) der Styrenlösungen PPO ($C_{PPO} = 4{,}5 \cdot 10^{-3}$ M/l; h = Stunden).

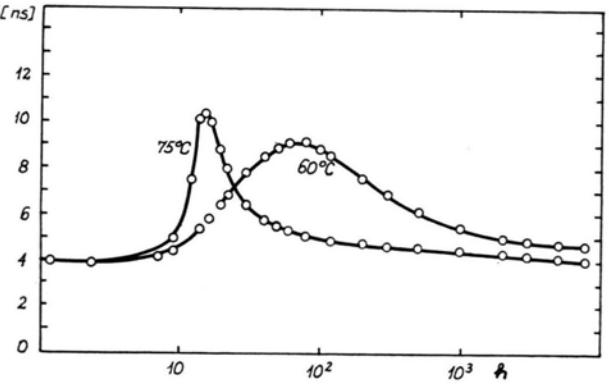

Abb. 2. Abhängigkeit der Szintillationsdauer (τ) von der Polymerisationszeit (t) der Styrenlösungen PPO ($C_{PPO} = 4{,}5 \cdot 10^{-3}$ M/l; h = Stunden).

Photostrom mit der in [1–5] beschriebenen Meßanordnung, b) aus der Lage des Maximums im Verteilungsspektrum der Impulsamplituden (wie in [6, 7]) bei Anregung mit Co-γ-Strahlung ermittelt. Beide Verfahren führten innerhalb der Fehlergrenzen zum gleichen Resultat (Abb. 1). Die Abklingzeiten τ – und zwar die schnelle Komponente – wurden mit einem in Anlehnung and ELLIOT und Mitarbeiter [8] gebauten Interferenz-τ-Meter gemessen [9]. Die Berechnungen der Szintillationszeiten erfolgten wie in der Arbeit von REICHEL [10]. Die Ergebnise in Abhängigkeit von der Polymerisationsdauer gibt Abb. 2 wieder.

2. *Diskussion der Ergebnisse*

Die untersuchten Lösungen stellen zeitabhängige 3-Komponentensysteme (Styrol, Polystyrol und PPO) dar. Nach BASILE [11] wird angenommen. daß das Verhältnis Monomer/Polymer die Radiolumineszenzausbeute und Abklingzeit bestimmt. Daher wurden beide Größen als Funktion des Konversionsgrades des Monomeren dargestellt. Es wurde angenommen, daß der Luminophor PPO in Anbetracht der geringen Konzentration den Polymerisationsprozeß nicht beeinflußt. Der

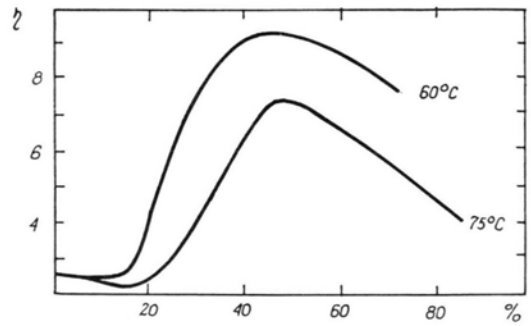

Abb. 3. Abhängigkeit der Radiolumineszenzausbeute (η) vom Konversionsgrad (%).

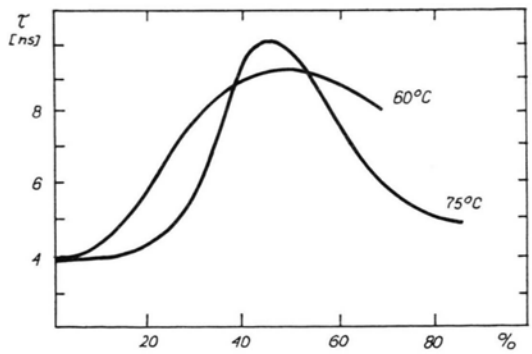

Abb. 4. Abhängigkeit der Szintillationsdauer (τ) vom Konversionsgrad (%).

Konversionsgrad wurde in Anlehnung an die Daten aus der Monographie [12] bestimmt (Abb. 3 und 4). Im Konversionsgradbereich $< 20\%$ ändert sich die makroskopische Zähigkeit der Lösungen sehr stark. Trotzdem sind die Änderungen von η und τ (Abb. 3 und 4) in diesem Bereich sehr gering. Das beruht wahrscheinlich auf der konträren Wirkung zweier konkurrierender Prozesse. Einerseits tritt durch die Umwandlung von Styrol in Polystyrol die Selbstlöschung des Styrols zurück, andererseits wird durch den Viskositätsanstieg die diffusionsbestimmte Energieübertragung vom Lösungsmittel zjum PPO behindert. Beide Effekte heben sich in ihrer Wirkung auf η und τ in diesem Bereich offenbar weitgehend auf.

Oberhalb eines Konversationsgrades von 20% steigen η und τ zu einem Maximum (bei etwa 50%) an. Dies ist auf weitere Abnahme der Selbstlöschung des Styrols zurückzuführen. Dafür spricht auch die Zunahme der Abklingzeit in diesem Gebiet. Die bei noch höheren Konversionsgraden beobachtete Abnahme von η und τ ist vorerst noch ungeklärt und soll weiter untersucht werden.

In der Endphase der Polymerisation nähert sich τ wieder dem Anfangswert ($\sim 3{,}9$ ns). Daher nehmen wir an, daß das PPO selbst seine Lebensdauer im Polymerisationsprozeß nicht ändert, die beobachteten Änderungen vielmehr auf Veränderungen im Energieübertragungsprozeß mit dem Polymerisationsgrad beruhen. In der Anfangs- und Endphase des Polymerisationsprozesses verläuft die Energieübertragung schnell nach dem Schema

$$M^* + L \rightarrow M + L^*,$$
$$P^* + L \rightarrow P + L^*.$$

(Der Stern kennzeichnet den angeregten Zustand.) Da die gemessene Szintillationsabklingzeit ($\sim 3{,}9$ ns) der von PPO (nach BERLMAN [13] 2,7 ns) sehr nahe kommt, wird ein direkter Energieübergang zwischen den beiden Partnern angenommen [14, 15]. Bei mittleren Konversionsgraden besteht ein komplizierterer Übertragungsmechanismus über monomere und polymere Moleküle nach dem Schema [16]

$$M^* + P \rightarrow M + P^* \rightarrow M^* + P,$$

bis ein Luminophormolekül erreicht ist. Das könnte zu einer Verlängerung der Szintillationsdauer führen.

Die vorliegenden Meßergebnisse stimmen quantitativ weitgehend mit den Ausbeutemessungen von BASILE [11] am System Styrol + Polystyrol übereini. Die Konvergenz der Radiolumineszenzausbeute von Szintillatoren, die bei verschiedenen Temperaturen polymerisiert wurden (die also verschiedene mittlere Molekulargewichte besitzen) zu einem Wert ist ein Beweis für die Schlußfolgerung von HEUSINGER [17], daß bei hohen mittleren Molekulargewichten die Radiolumineszenzausbeute vom Molekulargewicht des Lösungsmittels unabhängig ist.

[1] F. H. KRENZ, Trans. Faraday Soc. **51**, 2 [1955].
[2] A. WEINREB u. P. AVIVI, Liquid Scintillation Counting, London 1958.
[3] Z. POLACKI u. M. GRODEL, Proceedings of the International Conference on Luminescence, Budapest 1965.
[4] Z. POLACKI u. M. GRODEL, Acta Phys. Polon. **32**, 521 [1967].

[5] E. A. ANDREESCHCHEV, E. E. BARONI, K. A. KOVIRZINA, E. PANI, I. M. ROSMAN u. W. M. SCHONIA, Probory i Tekhnika Experimenta **1**, 32 [1956].
[6] J. ANDRUSZKIEWIECZ, W. KUŹMA u. Z. POLACKI, Nukleonika **5**, 575 [1960].
[7] I. M. ROZMAN u. S. E. KILIN, Uspiechi Fiz. Nauk **69**, 459 [1959].
[8] J. O. ELLIOT, S. M. LIEBSON, R. D. MYERS u. C. F. RAVILIOUS, Rev. Sci. Instrum. **21**, 631 [1950].
[9] M. GRODEL u. Z. POLACKI, Zeszyty Naukowe Politechniki Gdańskiej, Fizyka, **5**, 63 [1969].
[10] R. REICHEL, Kernenergie **3**, 1172 [1960].
[11] L. J. BASILE, J. Chem. Phys. **36**, 2204 [1962]; Trans. Faraday Soc. **60**, 1702 [1964].
[12] R. H. BOUNDY u. R. F. BOYER, Styrene, its Polymers, Copolymers and Derivatives, New York 1952.
[13] J. B. BERLMAN, Luminescence of Organic and Inorganic Material, ed. H. KALLMANN, New York 1962.
[14] F. WILKINSON, Luminescence in Chemistry, ed. E. J. BOWEN, London 1968.
[15] TH. FORSTER, Bioenergetics, Vol. **22**, Amsterdam 1967, S. 61–80.
[16] J. B. BIRKS u. J. C. CONTE, Proc. Roy. Soc. London A **303**, 85 [1968].
[17] H. HEUSINGER, Z. Naturforsch. **15 a**, 1068 [1960].

^{13}C-NMR Chemical Shift Anisotropy in Benzene-1-^{13}C

GERHARD ENGLERT

Physical Research Department
F. Hoffmann-La Roche & Co., Ltd., Basle

(Z. Naturforsch. **27 a**, 715—716 [1972]; received 2 February 1972)

The ^{13}C-NMR spectrum obtained by the pulsed Fourier technique, of benzene-1-^{13}C oriented in a nematic liquid crystal was analysed. From the chemical shift difference between the nematic and isotropic phase a value for the ^{13}C chemical shift anisotropy in benzene-1-^{13}C of +190 ppm was determined.

Recently, we reported the ^{1}H-NMR spectra of benzene and benzene-1-^{13}C in isotropic and nematic solution [1]. In the meantime we have investigated the ^{13}C-NMR spectra of benzene-1-^{13}C in both phases applying the pulsed Fourier NMR technique. It was the aim of this investigation to obtain information on the anisotropy of the ^{13}C chemical shift. A recent communication by YANNONI and BLEICH [2] on the ^{13}C shift anisotropy in polycrystalline benzene (^{13}C in natural abundance) at −40 °C prompted us to report our own results obtained by a different method.

The ^{13}C- and ^{1}H-NMR spectra of 38 mg of benzene and benzene-1-^{13}C in 450 mg of N-[p-ethoxybenzylidene]-p-n-butylaniline in a 5 mm o. d. tube were recorded at 22.63 and 90 MHz. The tube which was the same as previously used [1], was enclosed in a 10 mm o. d. tube containing D_2O to serve as a lock-signal. A Bruker HX 90/15 NMR spectrometer equipped with a Nicolet 1083 computer was used.

In the nematic phase the non-spinning sample yielded a ^{13}C spectrum which, as in the PMR case, is mainly determined by the direct dipolar couplings. The ^{13}C part of the spectrum, which is shown in the Fig. 1 (top), and the ^{1}H part, were both obtained by the pulsed Fourier technique at 24 °C (probe temperature). They were analysed using the computer program LAOCOONOR. The following indirect couplings (in Hz) were assumed [1]:

$$J_{HH}(\text{ortho}) = 7.54\,, \quad {}^1J_{^{13}CH} = 158.17\,,$$
$$J_{HH}(\text{meta}) = 1.38\,, \quad {}^2J_{^{13}CH} = 1.13\,,$$
$$J_{HH}(\text{para}) = 0.64\,, \quad {}^3J_{^{13}CH} = 7.62\,,$$
$$ {}^4J_{^{13}CH} = -1.16\,.$$

The direct couplings and their standard deviations (in Hz) iteratively obtained upon assignment of 104 transitions in the ^{13}C part and 62 transitions in the ^{1}H part of the spectrum were:

$$D_{HH}(\text{ortho}) = -307.14 \pm 0.08, \quad D_{^{13}CH} = -848.73 \pm 0.22,$$
$$D_{HH}(\text{meta}) = -58.72 \pm 0.10, \quad D_{^{13}C[C]H} = -116.57 \pm 0.15,$$
$$D_{HH}(\text{para}) = -38.41 \pm 0.15, \quad D_{^{13}C[CC]H} = -30.03 \pm 0.16,$$
$$D_{^{13}C[CCC]H} = -19.91 \pm 0.22.$$

The computer simulated spectrum (see Fig. 1, bottom) is in excellent agreement with the experimetal one. The RMS-deviation between observed and calculated transitions was 1.0 Hz. Assumption of a H–H (ortho) distance of 2.481 Å lead to the degree of order of the molecular C_6-symmetry axis:

$$S_{C_6} = -0.078\,.$$

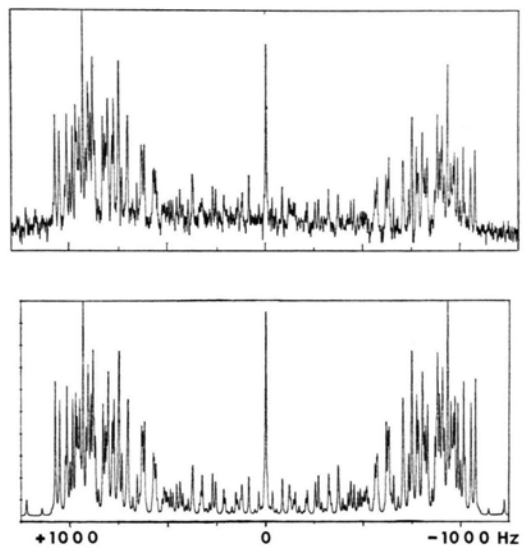

Fig. 1. Experimental and theoretical ^{13}C-NMR spectrum of benzene-1-^{13}C oriented in a nematic liquid crystal. *Top:* Experimental spectrum, obtained by pulsed (Fourier transform) NMR-technique. *Conditions:* 374 000 pulses of ca. 4 μsec, pulse repetition 0.68 sec (total measuring time 71 h), 4 K interferogram, exponential filtering (TC = −3), 24 °C, 22.63 MHz. *Bottom:* Computer simulated spectrum (for parameters used see text), half-width of the lines: 5.0 Hz.

The ^{13}C chemical shift (center of gravity of the symmetrical ^{13}C part) coinciding with the strong center line was arbitrarily chosen in the figure as 0 Hz.

In the isotropic phase the spectrum of the spinning sample under the condition of complete ^1H noise decoupling consisted of 14 singlets due to the 14 different (by symmetry) ^{13}C nuclei of the solvent. The total range of the chemical shifts was 3340 Hz (148 ppm). In the aromatic region a further slightly more intense singlet of benzene-1-^{13}C was observed. This singlet was shifted upfield compared to the center of the spectrum in the nematic phase. This implies that the ^{13}C and the ^1H shielding anisotropies are of opposite sign. If the components of the shielding tensor are denoted by $\sigma_{\parallel}$ and $\sigma_{\perp}$ for parallel and perpendicular orientation of the sixfold axis with the external field, values for the ^1H-anisotropy $\Delta\sigma = \sigma_{\parallel} - \sigma_{\perp}$ between -2.9 and -3.9 ppm have been reported for benzene [3, 4]. The possible sources of error encountered when measuring ^1H shielding anisotropies have been discussed by several authors [4–6]. The difficulties are expected to be considerably reduced, however, with ^{13}C-NMR because the observed shift differences between the two phases are usually larger. Actually, we observed:

$$\sigma_{NEM} - \sigma_{ISO} = -9.9 \pm 0.2 \text{ ppm}.$$

The ^{13}C anisotropy is given by:

$$\Delta\sigma = \tfrac{3}{2} \cdot (\sigma_{NEM} - \sigma_{ISO}) \cdot 1/S_{C_6} = +190 \pm 4 \text{ ppm}.$$

This value is in good agreement with the reported one of $+180$ ppm obtained in polycrystalline benzene [2].

The error stated above only takes into account the deviation from the mean of two independent measurements. Other sources of error might be the neglection of vibrational corrections to the observed D_{HH}(ortho)-coupling [1] ($\sim 4\%$), the small change in susceptibility between nematic and isotropic phase ($\sim$0.1 to 0.2 ppm) [6], and the temperature dependence of the chemical shifts [5] due to local shielding contributions. Although the total influence of these effects is difficult to estimate, we feel that the reported value for $\Delta\sigma$ is accurate to $\pm 10\%$.

[1] G. Englert, P. Diehl, and W. Niederberger, Z. Naturforsch. **26 a**, 1879 [1971].
[2] C. S. Yannoni and H. E. Bleich, J. Chem. Phys. **55**, 5406 [1971].
[3] G. Englert and A. Saupe, Z. Naturforsch. **19 a**, 172 [1964].
[4] J. Lindon and B. P. Dailey, Mol. Phys. **19**, 285 [1970].
[5] C. S. Yannoni, IBM J. Res. Devel. **15**, 59 [1971].
[6] A. D. Buckingham, E. E. Burnell, and C. A. de Lange, J. Amer. Chem. Soc. **90**, 2972 [1968].

The Critical Solution Points of Some Hydrocarbons in Deuterated Nitromethane *

Giorgio Spinolo and Paolo Ferloni

Institute of Electrochemistry, University of Pavia (Italy)

(Z. Naturforsch. **27 a**, 716—717 [1972]; received 11 January 1972)

As a part of our group research program on liquid systems containing hydrocarbons, the influence of nitromethane deuteration on the upper critical solution points (ucsp's) of binaries, where component **1** was nitromethane and component **2** was a ($C_5 - C_9$)-n. alkane, 1-octene or cyclooctane, was studied.

The apparatus and the adopted procedure were those previously described by Franzosini [1]. Fluka CD_3NO_2 (purum, $\geqq$ 99 at. % D), n. pentane (puriss., $\sim$ 99.98%), n. hexane (puriss., $\sim$ 99.96%), n. heptane (puriss., $\sim$ 99.87%), n. octane (puriss., $\sim$ 99.81%), n. nonane (puriss., $\sim$ 99.68%), 1-octene (puriss., $\geqq$ 99.7%) and cyclooctane (purum, $\geqq$ 98%) were employed.

The demixing curves we obtained are shown in Figures 1 and 2.

In the investigated composition ranges, the liquid-liquid equilibrium temperatures could be generally detected with a very satisfactory degree of accuracy, each measurement being, as a rule, reproducible within a few hundredths of a °K. Only for the (CD_3NO_2 + n. heptane)-system the boundaries of the miscibility gap could be drawn in a merely approximate way, owing to the fact that in most samples the demarcation line between the two liquid phases was nearly evanescent.

In Table 1 the ucsp co-ordinates of the binaries where **1** = CD_3NO_2 and **2** = n. alkane are summarized with those reported in recent literature for the corresponding binaries where **1** = CH_3NO_2.

Table 1. Coordinates of the ucsp's in binaries where **2** = n. alkane.

component **1**	component **2**	$N_{2,\max}$	$T_{\max}$ (°K)	Ref.
CD_3NO_2	n. pentane	0.43 ±0.01	372.0	this work
	n. hexane	0.37_5 ±0.01	376.8	
	n. heptane	0.33_5 ±0.01	$382._3$	
	n. octane	0.31 ±0.01	388.9	
	n. nonane	0.28 ±0.01	395.1	
CH_3NO_2	n. pentane	0.45 ±0.01	370.7	2
	n. hexane	0.41_5 ±0.01	375.4	3
		0.3775	375.55	4
	n. heptane	0.36 ±0.005	381.0	3
		0.350	381.45	4
	n. octane	0.33 ±0.01	387.2	3
		0.315	387.65	4
	n. nonane	0.30_5 ±0.005	393.8	3
		0.280	393.45	4

Reprint requests to Prof. Paolo Franzosini, Istituto di Elettrochimica – Università, Viale Taramelli 16, *I-27 100 Pavia*, Italy.

* The financial aid of the Italian National Research Council (Rome) is acknowledged.

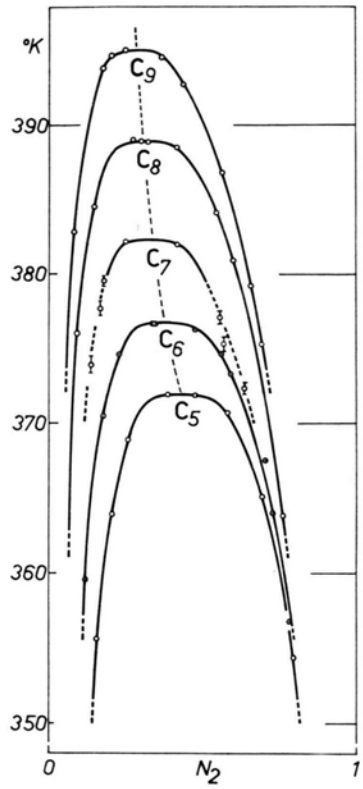

Fig. 1. Miscibility gaps in binary mixtures of trideuteronitromethane with (C_5-C_9)-n. alkanes.

The comparison between the two sets of data allows to conclude that, in each couple of corresponding binaries, the main effect of nitromethane deuteration is to raise up the ucsp temperature by an amount averaging 1.3 °K. This temperature effect is similar to that observed by RICCARDI et al. [2] in mixtures formed with the same n. alkanes and acetone or hexadeuteroacetone, respectively.

It seems moreover that, component **2** remaining the same, the $N_{2,\max}$ value tends to be lowered by substituting CH_3NO_2 with CD_3NO_2, though this composition effect is apparent only when the comparison is restricted to the data from Refs. [2] and [3], which were taken by employing the same apparatus and procedure we adopted: anyway, the fact that MALESINSKA [4] (in order to obtain an easier detection of demixing) added some methylene blue to nitromethane is also to be mentioned.

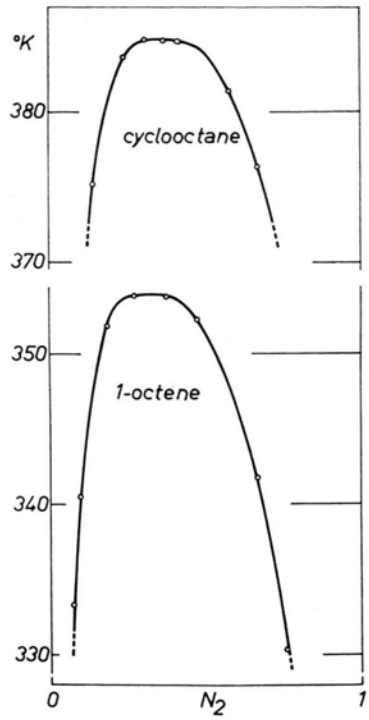

Fig. 2. Miscibility gaps in binary mixtures of trideuteronitromethane with 1-octene and cyclooctane.

Table 2. Coordinates of the ucsp's in binaries where **2** = 1-octene or cyclooctane.

component **1**	component **2**	$N_{2,\max}$	$T_{\max}$ (°K)	Ref.
CD_3NO_2	1-octene	$0.31_5 \pm 0.01$	354.0	this work
	cyclooctane	0.37 ± 0.01	384.8	
CH_3NO_2	1-octene	0.33 ± 0.01	351.9	[5]
	cyclooctane	$0.39_5 \pm 0.01$	382.7	[2]

Concerning the systems containing 1-octene and cyclooctane (see Table 2), it may be finally observed that, the composition effect remaining approximately the same as before, the ucsp temperature increase is larger by a factor ~ 1.6.

The authors are grateful to Mr. M. BALDI for his help in preparing the samples.

[1] P. FRANZOSINI, Z. Naturforsch. **18 a**, 224 [1963].
[2] R. RICCARDI, P. FRANZOSINI, and M. ROLLA, Z. Naturforsch. **23 a**, 1816 [1968], and private communication of unpublished data.
[3] M. ROLLA, P. FRANZOSINI, R. RICCARDI, and L. BOTTELLI, Z. Naturforsch. **22 a**, 48 [1967].
[4] B. MALESINSKA, Bull. Acad. Pol. Sci., Sér. Sci. Chim. **8**, 53 [1960].
[5] P. FERLONI, A. GEANGU-MOISIN, P. FRANZOSINI, and M. ROLLA, Z. Naturforsch. **26 a**, 1713 [1971].